THE JOURNAL OF PHYSICAL CHEMISTRY C
A JOURNAL OF THE AMERICAN CHEMICAL SOCIETY

pubs.acs.org/JPCC

Article

Hydration of Hydroxylated and Fluorinated Synthetic Micas Exchanged with Monovalent Cations: A NAP-XPS and Molecular Dynamics Investigation

Laurent J. Michot, Loïc Guérin, Théophane Bernhard, Ayumi Koishi, Francis Claret, Eric Ferrage, Jean-Jacques Gallet, Fabrice Bournel, and Virginie Marry*

Cite This: *J. Phys. Chem. C* 2026, 130, 11831−11846

Read Online

ACCESS | Metrics & More | Article Recommendations | Supporting Information

ABSTRACT: In order to better understand the wettability of mica minerals, we combined molecular simulations with near-ambient pressure XPS measurements of the early hydration stages of phlogopite mica containing either structural OH atoms or structural F atoms, for various monovalent compensating cations. The evolution of the environment of the atoms constituting the system (structural atoms, counterions, and water molecules) was studied as a function of increasing relative humidity. The evolution with relative humidity of the NAP-XPS component of O assigned to liquid water was considered as representative of a water adsorption isotherm. At low RH (≤0.2), fluorinated samples display significantly lower water adsorption than their hydroxylated counterparts, which agrees with a delay in hydration of surface cation for the fluorinated samples, evidenced by NAP-XPS. In parallel, alchemical transformations at different surface water contents were performed using molecular dynamics. This allowed calculating for two different micas the ratio between relative humidities for a given surface water amount. In the case of mica−OH, simulations showed that the surface with Na^+ is always more hydrophilic than that with Cs^+. For mica-F, the Cs^+ sample appears to be more hydrophilic at low hydration states (≤≈0.5 monolayer of adsorbed water), while the opposite is observed for higher amounts of adsorbed water. It may be that at low surface coverages, the interactions between fluorine and small Na cations are stronger than with Cs^+. Despite the uncertainties associated with both the NAP-XPS experiment and the force field used in simulations, the comparison between experiments and simulations yields good agreement at high relative humidity and minor discrepancies at low relative humidity. The hydrophilic/hydrophobic nature of the surface appears to strongly depend on the very first hydration stages, i.e., on the balance between cation/surface and cation/water interactions.

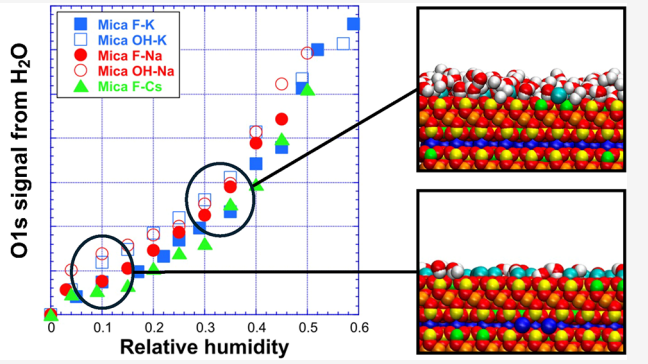

INTRODUCTION

Surface hydration is of prime importance in numerous scientific fields, ranging among others from biology,[1,2] catalysis,[3] biomaterials design,[4] or atmospheric chemistry.[5,6] Hydration phenomena are also crucial in the behavior of the so-called critical zone, i.e., "the heterogeneous, near-surface environment in which complex interactions involving rock, soil, water, air, and living organisms regulate the natural habitat and determine the availability of life-sustaining resources."[7] For this reason, a vast body of literature has been devoted to the interaction of water with various mineral surfaces present in the critical zone,[8] with numerous works devoted to the case of phyllosilicates that are especially reactive toward water, and control to a large extent soil stability, plant nutrition, and contaminant transport in the critical zone. Phyllosilicates are lamellar aluminosilicates that are ubiquitous in the subsurface. Depending on their structure, they can be either swelling or nonswelling. The former type of structure corresponds to the family of smectites and vermiculites whose hydration properties have been studied for decades through a combination of experimental and simulation techniques that have focused on understanding the structure and dynamics of bidimensional confined water.[9−15] The latter type comprises uncharged minerals such as kaolinite, talc, chlorite, or pyrophyllite, and charged ones, i.e., micas. As far as micas are concerned, their hydration in aqueous solutions has been extensively studied using the surface force apparatus (SFA),[16,17] atomic force microscopy (AFM),[18,19] or X-ray reflectivity measure-

Received: June 8, 2026
Revised: July 27, 2026
Accepted: July 28, 2026
Published: August 7, 2026

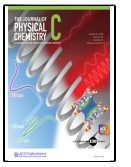

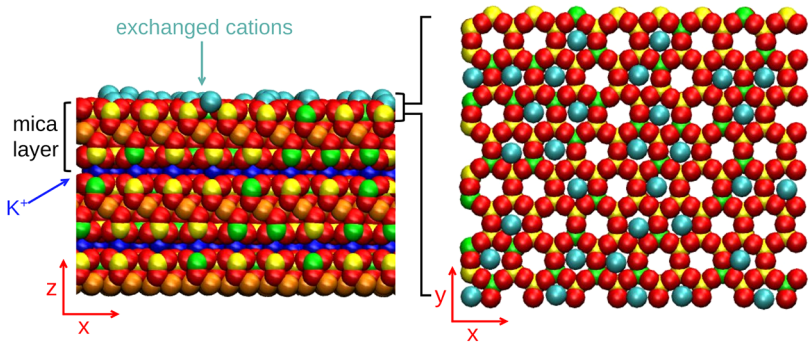

Figure 1. Snapshot of mica layers. Left: three layers stacked on top of each other with natural K^+ counterions between them (dark blue atoms). Surface-exchanged cations (cyan atoms) are located on the surface of the lamellar stacks. Right: Top view of the stack (for clarity, only surface Si, Al, and O atoms are represented). In the dry state, most of the cations are located above the ditrigonal cavities. Red: O, yellow: Si, green: Al, and orange: Mg. The OH/F groups, located within the layer, are not visible in this snapshot.

ments,[20−23] as these minerals exhibit macroscopic smooth planar surfaces, which has allowed examining the structure of the electrical double layer at their surfaces and evidencing the existence of hydration forces. A few experiments were also devoted to the investigation of hydration layers on micas in humid atmospheres using either SFA[24] or AFM.[25] Much less work has been devoted to the first hydration stages of mica surfaces. This is in part due to experimental issues. Indeed, unlike with swelling minerals that bear a very high water adsorption capacity, the surface available for water adsorption in the case of micas is rather limited, which somehow impairs the use of classical techniques such as infrared spectroscopy or neutron scattering. Experiments based on interferometry were carried out to obtain a quantitative view of the first stages of water adsorption on cleaved micas exchanged with K^+ or H^+[26] and revealed the importance of cation hydration in the process. In parallel, molecular simulations were used in a few studies to analyze the structure and dynamics of water at the mica surface with increasing relative humidity (RH)[23,27−31] and for different surface ions, but experimental collation of simulation data was not carried out. X-ray photoelectron spectroscopy is a surface-sensitive experimental technique that provides information about the chemical bonding of elements. It has been used for studying various silicate minerals, including micas,[32−36] and was recently combined with AFM to analyze the hydration of various micas.[37] However, until recently, XPS experiments could only be performed under high vacuum, which precludes analyzing the adsorption of various species in situ, and, for instance, data in ref 37 were obtained in the dry state and in a so-called hydration state without any control over RH. The introduction of near-ambient pressure XPS (NAP-XPS)[38−40] around two decades ago significantly transformed the landscape of surface science. Indeed, NAP-XPS systems can operate under pressures of up to approximately 20 mbar, which allows performing experiments up to 100% RH for temperatures below approximately 7 °C. This was applied to the study of aqueous electrolyte suspensions[41−43] as well as to the hydration of smectites[44] and layered double hydroxide surfaces.[45] In the present paper, we use NAP-XPS to analyze the first stages of water adsorption for RH ≤ 60% on mica surfaces exchanged with monovalent cations with different hydration enthalpies, i.e., Na^+, K^+, and Cs^+. We concentrate on the signals corresponding to the solid, the surface ions, and water molecules. In addition to the effect of the nature of the surface compensating cation, in line with the work carried out in ref 23 we also analyze the behavior of synthetic mica samples for which structural hydroxyl groups have been replaced by fluorine atoms. Indeed, in the case of other phyllosilicates, such structural substitution has been shown to affect the hydrophilic/hydrophobic nature of the surface.[46−48] In parallel, molecular dynamics simulations are performed to analyze the evolution with relative humidity of water uptake on the various mica samples. The collation between experimental and simulated results provides information on the main parameters controlling mica/water interactions.

MATERIALS AND METHODS

Sample Preparation

Synthetic hydroxylated and fluorinated phlogopite micas were used in this study. Their structural formulas can be written as $K_2(Si_6Al_2)Mg_6O_{20}(OH,F)_4$. Samples were cleaved by using scotch tape to generate fresh surfaces. Surface cation exchanges were carried out by contacting the cleaved surface of the pristine mica with 1 M solutions of KCl, NaCl, or CsCl three times. The surfaces were then rinsed with Milli-Q water at least 10 times to remove any excess salt. The final samples were kept protected from an ambient atmosphere to avoid any contamination. A molecular representation of mica layers with their natural K^+ counterions and the counterions exchanged at the surface after rinsing and drying is shown in Figure 1. Since mica is a nonswelling material, only the cations located on the surface of the particle are exchanged, while the cations located between the layers within the mica particle remain K^+. In the top view, one can see the ditrigonal cavities formed by the Si and O hexagons on the surface of the mica layer. Some of these are occupied by the surface cations.

The samples were then glued onto specific sample holders using silver varnish and transferred to the preparation chamber available on the NAP-XPS of Sorbonne Université set on TEMPO beamline at Synchrotron SOLEIL. This station utilizes a SPECS PHOIBOS NAP-XPS 150 analyzer for the measurements.[43,44] In order to maximize the photoelectron signal intensity, the analyzer aperture (a pinhole 0.3 mm in diameter) is placed close to the sample surface at a distance of ∼0.3 mm. All spectra were obtained using an incident energy of 980 eV at a pass-energy of 50 eV with a slit of 3 mm × 20 mm, corresponding to an analyzer resolution of 500 meV. During the beamtime, 5 samples could be analyzed, i.e., fluorinated micas exchanged with Na^+, K^+, and Cs^+ and hydroxylated micas exchanged with Na^+ and K^+. They will be

https://doi.org/10.1021/acs.jpcc.6c03757
J. Phys. Chem. C 2026, 130, 11831−11846

referred to as Mica−F-Ct and Mica−OH-Ct, where Ct stands for the exchange cation.

NAP-XPS Experiments

After introduction into the NAP-XPS analysis chamber, the samples were cooled down to a temperature of ≈6 °C using a Peltier cooler. Ultrapure degassed water was then introduced through a leak valve. For each sample, around 10 values of water pressure were used, corresponding to relative humidities ranging between ≈5 and ≈60%. For each pressure value, broad spectra were first recorded to assess the quality of the signal. High-resolution spectra on various spectral regions corresponding to different chemical elements of interest were then acquired, with acquisition conditions adjusted for reaching acceptable signal/noise ratios. Under the conditions used in the present study, no drastic effects linked to beam damage were observed, and we then considered that the mica layers maintained their integrity during the whole analysis.

Micas, being semiconductors, accumulate charge under X-ray irradiation, which increases the apparent binding energy of core levels[49] and widens the peaks. With increasing water pressure, such detrimental effects tend to vanish due to the presence of stray electrons generated by the X-ray beam in water vapor, which discharges the sample surface.[39] In order to correct these shifts that change with pressure, we focused on the position and width of the Mg 2p peak. The position and width of this peak evolve with water pressure and reach constant values around 49 and 1.5 eV, respectively, for all of the samples for RH ≥ 50%. As such binding energy value is close to that found in brucite (49.3 eV[50]) or hydrotalcite (48.8 eV[51]), we decided to correct all of the spectra by fixing the position of the Mg 2p peak at its value at the highest RH recorded for each sample and shifting all values accordingly. It must be pointed out that by applying such a correction, the primary aliphatic C−C component of the C 1s spectrum, associated with contamination, is observed at 284.6 eV. Such a value concurs with the accepted binding energy for contamination carbon, i.e., 284.8 eV,[52] which provides further validation of the correction based on Mg that we applied. After removing the background using a Shirley profile, the spectra were fitted using sums of Gaussians. The spin−orbit splitting values were set to 0.4 eV for the Al $2p_{1/2}/2p_{3/2}$ doublet, 0.6 eV for the Si $2p_{1/2}/2p_{3/2}$ doublets, 2.3 eV for the Cs $4d_{3/2}/4d_{5/2}$ doublet, 2.7 eV for the K $2p_{1/2}/2p_{3/2}$ doublet, and 13.9 eV for the Cs $3d_{3/2}/3d_{5/2}$ doublet. Mg 2p was modeled with a single Gaussian component, owing to the small spin−orbit splitting of 0.28 eV.[53] The maximal accepted full width at half-maximum (FWHM) at high RH, i.e., when charge effects are minimal, was fixed at 1.5 eV. When a Gaussian component was found to have a too high fwhm at high RH, an additional component was added. The number of components used for fitting was then fixed at high RH, i.e., when charge effects are minimal. At low relative pressures, the same number of components was used, and higher band widths (up to 3.5 in the worst cases) could be used.

Molecular Simulations

Initial configurations of phlogopites were created, containing two layers of 8 × 4 = 32 unit cells of formula $K_2(Si_6Al_2)$-$Mg_6O_{20}(OH,F)_4$. One surface of the layer was artificially moved away from the other (with half the cations on each side to maintain local electroneutrality), in order to expose the surface on which the water will be adsorbed, as represented in the snapshot of Figure S1. The distance between the two surfaces was fixed to 120 Å, which is considered high enough to neglect interactions between the two surfaces. Water molecules were then added to the surface. The potassium cations located at the surfaces could be replaced by either Na^+ or Cs^+ in order to simulate phlogopite exchanged with different cations.

The hydrophilicity of a surface can be evaluated by calculating the work of adhesion, which is defined as the work per unit area required to remove a liquid from the solid surface. The greater the work of adhesion, the more hydrophilic the surface. We used the thermodynamic cycle schematized in Figure 2 to calculate the differences in work of adhesion between the samples differing by the cation adsorbed on the surface or by the presence or absence of fluorine in the cell.

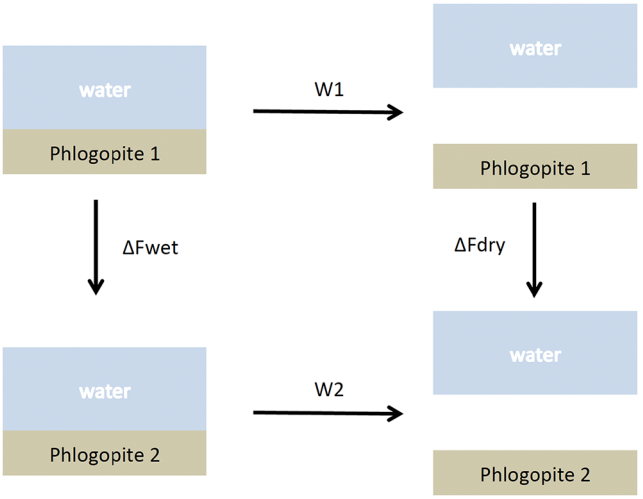

Figure 2. Thermodynamic cycle used to calculate differences in work of adhesion.

$\Delta W = W_2 - W_1$ can be obtained from the difference between ΔF of the alchemical transformation of system 1 into system 2 in the dry and wet states: $\Delta W = \Delta F_{dry} - \Delta F_{wet}$. The principle of an alchemical transformation is to gradually change the configurational energy $V = \lambda V_1 + (1 - \lambda)V_2$ by slowly varying λ from 1 to 0 during a single molecular dynamics run of duration T. The free energy difference between state 1 and state 2 can be estimated by calculating

$$\int_0^T \frac{d\lambda}{dt}\frac{\partial V(\lambda)}{\partial t}dt = \int_0^T \frac{d\lambda}{dt}(V_1 - V_2)dt \quad (1)$$

$V_1 - V_2$ can be calculated at each time step as the difference between the energies of the configuration at time t, calculated with the interaction potentials of state 1 and the interaction potentials of state 2. This method was already used in our previous work on talc[54] and was shown to be more accurate than measuring contact angles. Furthermore, in this case, the surfaces being hydrophilic, water spreads over the surface, and contact angles cannot be easily calculated. Before performing alchemical transformations, the initial boxes of the simulations with Cs^+ as surface cation were equilibrated both in the dry state and after addition of 25 H_2O per cation. This latter value corresponds to a layer of water adsorbed on the surface with a thickness of 15 Å, i.e., the equivalent of 5 water layers. At this distance, water at the interface with the vapor phase can be considered to be negligibly influenced by the mica surface.

https://doi.org/10.1021/acs.jpcc.6c03757
J. Phys. Chem. C 2026, 130, 11831−11846

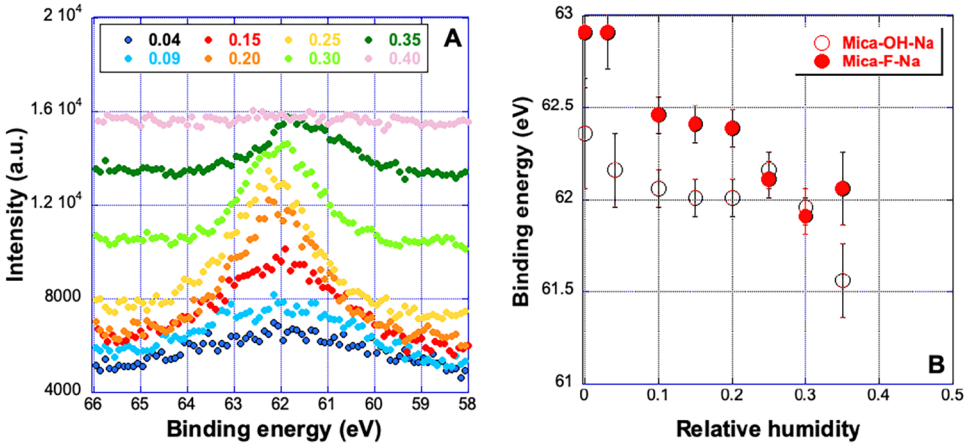

Figure 3. Evolution with relative humidity of (A): Na 2s NAP-XPS spectra for Mica−OH-Na and (B): position of the Na 2s peak for Mica−OH-Na and Mica−F-Na.

Simulations were performed using the LAMMPS code,[55] with a time step of 1 fs. The original clayFF force field was chosen to calculate the interatomic interactions (for clay and cations).[56] SPC/E water model was used.[57] The clay layers were allowed to relax horizontally (a pressure of 1 bar was imposed along directions x and y), the vertical dimension of the box remaining fixed to 120 Å. The temperature was fixed at 300 K. After a phase of equilibration of several hundreds of ps, alchemical transformations of 4 ns were performed for transforming surface Cs^+ into Na^+, and Cs^+ into K^+ in the dry and hydrated states. In this case, only the Lennard-Jones parameters between the cation and the rest of the system changed from system 1 to system 2. The transformation of mica−OH into mica-F was a little more complicated because the hydrogen atoms of the hydroxyl group must be deleted at the same time, as the charge and the Lennard-Jones parameters of O (transforming into F) are modified. During the alchemical transformation, the harmonic bonds between O/F and H were maintained to counteract the side effects of atom annihilation. As shown in Fleck et al.,[58] it has no impact on free energy calculation. The alchemical transformations were performed to change mica−OH into mica-F for each surface cation. It was verified that the obtained free energies were almost independent of the initial configuration: 6 alchemical transformations were performed starting from 6 initial configurations obtained at several tens of ps intervals along long simulations of dry and wet phlogopite with Cs. The free energy differences were found to be less than 1 per 1000. It was also verified that increasing the duration of the alchemical transformation did not change the results, which indicates that 4 ns is sufficient for the alchemical transformation. On one of the hydrated systems, we also verified that the result was the same when the inverse transformation was carried out. Moreover, the alchemical transformation of K^+ into Na^+ was also performed for mica−OH in order to check that the obvious relationship $\Delta W(Cs \rightarrow Na) = \Delta W(Cs \rightarrow K) + \Delta W(K \rightarrow Na)$ was well verified.

RESULTS AND DISCUSSION

Surface Cations

Sodium. As shown in Figure 3A in the case of Mica−OH-Na, spectra obtained in the Na 2s region display very weak peaks with a low signal/noise ratio. Figure 3B displays the evolution of the binding energy of the Na 2s peak as a function of relative humidity (RH). In the case of both micas, for relative humidity higher than 40%, no signal corresponding to Na 2s is observed. Such a vanishing of the Na signal has already been observed in NAP-XPS studies of swelling clays[59,60] and was assigned to the NAP-XPS measurement itself, which resulted in a displacement of the hydrated ions initially located at the surface due to the beam. Indeed, moving the X-ray spot on the sample allowed recovering an observable Na signal that vanished with time under the beam.

Both samples exhibit higher binding energies than those observed for hectorite and saponite,[60] the former being located at a higher energy than the latter. This strongly suggests that the local charge felt by the surface sodium ion shifts its binding energy toward lower values. Indeed, the structural charge of micas is higher than that of swelling clays and is located in the tetrahedral layer. Furthermore, Mica-F exhibits a slightly higher Na 2s binding energy than Mica−OH across the range of relative humidity where Na^+ ions are still close to the surface. It could be explained by changes in the electrostatic properties resulting from the presence of fluorine in the layer. Simulations show that, regardless of the type of mica, the vast majority of counterions are located above the ditrigonal cavities (hexagons formed by Si−O−Si), that is, above the OH/F groups situated inside the cavities (see Figures 1 and S2). While the O atoms in the OH groups and F groups are located fairly deep within the layer, the H atoms in the OH groups point toward the cation and may alter its electrostatic environment. The influence of OH/F groups can be observed on the radial distribution functions between Na and surface oxygen atoms (Os) obtained by simulation in the dry state (see Figure S3): they show peaks that are close in position (about 2.4 Å), but their shapes are quite different. Moreover, in the case of mica-F, all Na^+ ions are located above the ditrigonal cavities, whereas in the case of mica−OH, a small fraction of the Na^+ ions are located above Al atoms (see Figure S2), which shows that the position above the cavities is not necessarily the most favorable.

For both samples, an increase in RH appears to shift the binding energy downward by ≈−1 eV. Such a decrease with a similar value was observed previously[60] in the case of swelling clays and can be assigned to Na^+ hydration. The data displayed in Figure 3B could suggest that such a shift occurs for lower relative humidity in the case of Mica−OH compared to Mica-

https://doi.org/10.1021/acs.jpcc.6c03757
J. Phys. Chem. C 2026, 130, 11831−11846

F, which may suggest a delay in hydration for the fluorinated sample.

Indeed, this is what we see in the radial distribution function between Na and Os in Figure S3: While the $g(r)$ functions are very similar for dry mica-F and mica-F hydrated with 1 H_2O per Na^+, the first peak shifts toward larger distances even at low hydration states in the case of mica−OH, indicating that Na^+ moves further away from the surface under the influence of water. It is confirmed by the cationic distributions in the direction perpendicular to the surface obtained in mica−OH (Figure 4): some Na ions move away from the surface as soon as a very small amount of water is present. This results in the appearance, under the action of water, of a distribution peak approximately 1 Å further from the surface than the peak closest to the surface, which is the main peak at a water-to-cation ratio of 6. This change in the Na^+ environment may, on the one hand, explain the decrease in binding energy. On the other hand, it is possible that Na^+ ions, being further away from the surface, have higher freedom of motion, which could explain the displacement of cations under the beam. It should be noted, however, that unlike less-charged clays,[61,62] fully hydrated Na^+ ions (outer sphere complexes, seen at a distance of 8 Å from Mg on the blue dashed line) were rarely observed during the simulations, even in the state corresponding to 25 H_2O molecules per cation, which is in agreement with Koishi et al.[23] Thus, the proportion of fully hydrated Na remains low.

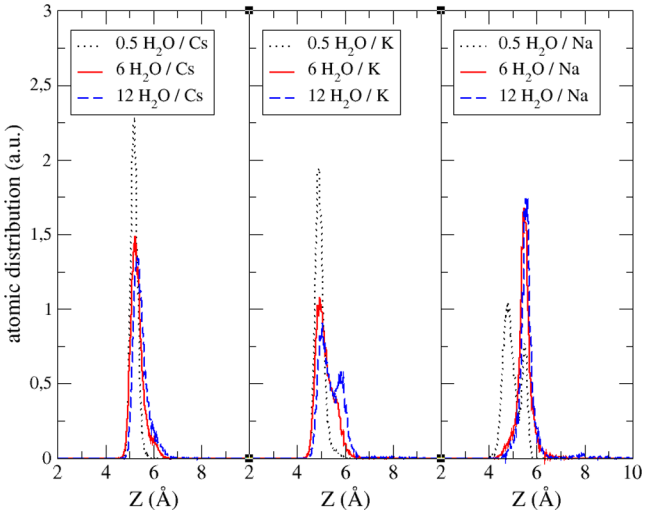

Figure 4. Evolution of cationic distributions with the number of water molecules adsorbed onto the surface. Left: mica−OH-Cs, middle: mica−OH-K, and right: mica−OH-Na. z = 0 corresponds to the location of Mg atoms (the middle of the clay layer).

Cesium. As mentioned in the Materials and Methods section, due to time constraints, only the fluorinated mica exchanged with Cs could be analyzed. Still, as the hydration energy of Cs^+ is significantly lower than that of most cations, it is relevant to examine its behavior, to compare it with surfaces with other cations. Figure S4 shows the spectra obtained in the energy region corresponding to the doublet Cs $3d_{5/2}$-Cs $3d_{3/2}$ that is barely visible for high RH. Figure 5 displays the evolution with RH of the binding energy of the Cs $3d_{5/2}$ (Figure 5A) and Cs $4d_{3/2}$ (Figure 5B) signals. At low RH, the signal corresponding to Cs $4d_{3/2}$ is strongly affected by its proximity to the Al 2p signal, and the values derived from fitting are then rather uncertain. If one excepts the first two points, the positions of both the Cs $3d_{5/2}$ (Figure 5A) and Cs $4d_{3/2}$ (Figure 5B) signals remain approximately constant regardless of the RH, which can be linked to the low hydration energy of Cs^+. The binding energy corresponding to Cs $4d_{3/2}$ is close to that observed for hectorite and saponite,[60] which seems to suggest that Cs^+ is only marginally affected by its surface environment.

In fact, simulations show that hydration has little effect on the Cs distributions, whose peak remains at the same distance from the surface (Figure 4). Cs^+ remains localized above the ditrigonal cavities when the amount of water on the surface is increased, indicating a strong affinity for the mica surface compared to Cs^+ affinity for water. Nevertheless, the presence of water broadens the distribution peak toward longer distances (which is also shown by the radial distribution function between Cs and the surface oxygen atoms—not shown here), indicating that Cs^+ ions deviate slightly from their positions in the dry state when they are hydrated. Similarly, the number of water molecules in their first hydration sphere increases until it plateaus at approximately 5 water molecules, which should be expected to change the binding energy. It is

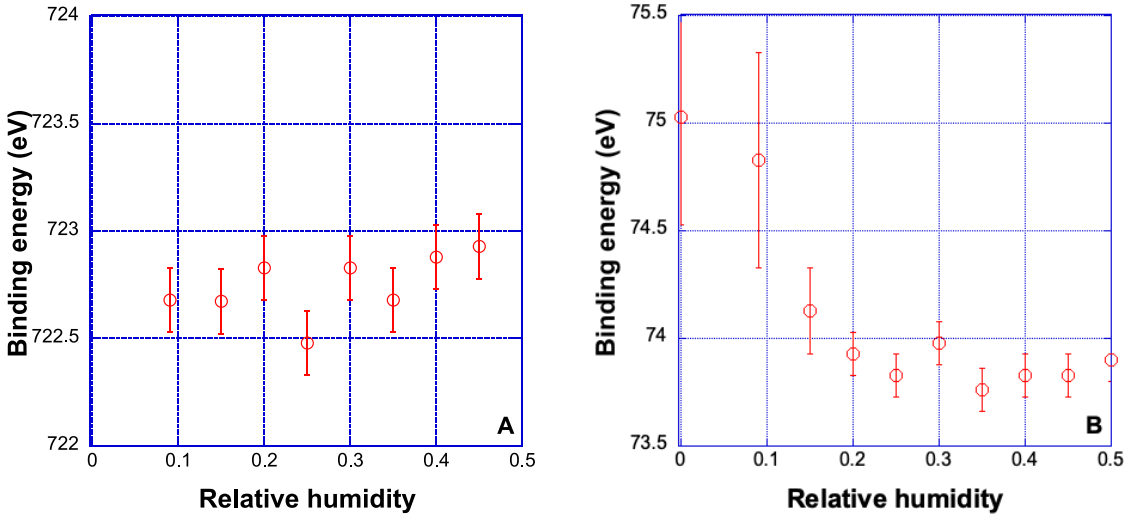

Figure 5. Evolution with relative humidity of the position of (A): the Cs $3d_{5/2}$ signal and (B): the Cs $4d_{3/2}$ signal.

https://doi.org/10.1021/acs.jpcc.6c03757
J. Phys. Chem. C 2026, 130, 11831−11846

possible that the effect of the surface on the binding energy is so significant that the effect of hydration is masked by its slight displacement from the surface.

Potassium. The case of potassium is somewhat complicated for two reasons. (i) Structural potassium is present in all samples, and (ii) the energy range corresponding to K 2p is affected by the presence of carbon contamination. Figures S5–S9 display the fitted spectra obtained for all micas. By comparing samples that bear only structural K with those in which the exchanged cation is K^+, it is possible to distinguish the signal corresponding to surface potassium ions that appears as an additional doublet located at a lower binding energy than structural potassium. The average position for structural potassium for the 5 samples is around 292 eV at high RH, whereas that corresponding to surface potassium is located around 290 eV. Figure 6 presents the evolution with relative humidity of the K $2p_{3/2}$ signal located around 290 eV for both Mica–OH-K and Mica–F-K.

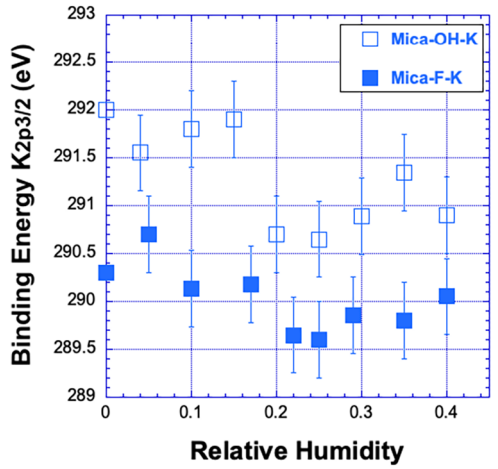

Figure 6. Evolution with relative humidity of the position of the surface K $2p_{3/2}$ signal for mica–OH-K and mica–F-K.

First, the average value for Mica-F is lower than that for mica–OH, which is opposite to what was observed for Na. In the case of K-substituted micas, the radial distribution functions between K and the surface oxygen atoms (not shown here) are very similar, with a first peak at a distance of 2.85 Å, which is slightly narrower in the case of mica-F. Furthermore, no cations are found outside the ditrigonal cavities, unlike in the case of Na. These differences, which indicate varying behavior depending on the cation, might explain why the bond energies do not follow the same trend depending on the OH/F group.

Second, as in the case of sodium, the evolution with relative humidity reveals a downward shift that can be assigned to hydration. However, this observation should be interpreted with caution, given the error bars and the fact that the first three data points at low relative humidity for mica–OH-K correspond to a very broad signal affected by carbon contamination (Figure S6). Nevertheless, simulations show that potassium also hydrates in the same way as sodium, which results in the appearance of a second distribution peak in Figure 4, although this peak is less intense and corresponds to higher amounts of water adsorbed on the surface. The fact that K^+ ions partially move away from the surface could explain this decrease in the binding energy.

This NAP-XPS analysis of exchange cations confirms that the technique allows for following their hydration and reveals differences linked to both the hydration behavior of the ion and the F/OH substitution in the layer. To some extent, experimental observations can be interpreted in light of the simulations, but the evolution of binding energies must take into account a set of factors that can only be qualitatively linked to what is observed in simulations. In the following section, we examine the influence of humidity and the nature of the F/OH groups on the structural atoms of the mica layers.

Structural Atoms. *Silicon.* The Si 2p spectra for all samples are broad and suggest the presence of multiple components. The energy range for Si 2p signals is consistent with values found in the literature for phyllosilicates in vacuum.[32−36] The position of the Si 2p peak is linked to the total charge of the structure. Indeed, the Si 2p XPS signal for talc, a noncharged phyllosilicate, is located at a binding energy that is 1 eV above that observed for vermiculite, a charged mineral.[34] Furthermore, in a study by X-ray photo-emission electron microscopy (X-PEEM) of swelling clay minerals with variable charge, Vantelon et al.,[63] observed various components in the Si 2p peak, the position of which could be related to both the total layer charge and charge location in the structure. In the case of low-charge hectorite that bears an octahedral substitution, signals centered around 103 and 102 eV were observed, whereas for low-charge saponite that bears a tetrahedral substitution, signals centered around 102 and 101 eV were observed. An increase of charge in saponite leads to the appearance of a third component located around 100 eV. These three components were assigned to silicon atoms bound through oxygens to 0, 1, or 2 Al atoms (the case of 3 Al being negligible). In the case of micas, it then seemed natural to fit the spectra with three components, corresponding to the same assignment. The fits for mica–OH-Na are shown in Figure 7. The fits obtained for the other micas are available in the Supporting Information (Figures S10–S13).

The proportions corresponding to these various Si sites can be estimated theoretically by randomly substituting Al atoms for Si atoms on the surface of a layer in such a way that the Loewenstein's rule is satisfied (no two Al atoms can be adjacent) and then calculating the proportion of Si atoms surrounded by 0, 1, 2, or 3 Al atoms. We performed this exercise on a large number of random configurations and obtained the following proportions: 28% of Si surrounded by 0 Al, 47% by 1 Al, 21% by 2 Al, and 4% by 3 Al. We observe that the proportion of Si surrounded by 3 Al is small and can be neglected. Figure proportions display the experimentally determined relative proportions of the 3 fitted signals together with the theoretical value represented by a dashed black line in Figure 8. Though not perfect, the match between experimental and calculated values is rather satisfactory, considering the potential errors in the fit and the assumptions underlying the calculation made (in addition to Loewenstein's rule, the sites where the Al are positioned are all equally likely).

To enforce the assignment of the various Si signals, it is very relevant to plot the evolution of their positions with increasing relative humidity (Figure 9).

It appears that the high-energy component does not vary with hydration, regardless of the sample. The medium-energy component appears to be roughly constant when the exchangeable cation is either K^+ or Cs^+. In the case of Na^+, a slight evolution toward higher wavenumbers can be observed that is similar for the F- and OH-micas. Finally, the lower-

https://doi.org/10.1021/acs.jpcc.6c03757
J. Phys. Chem. C 2026, 130, 11831−11846

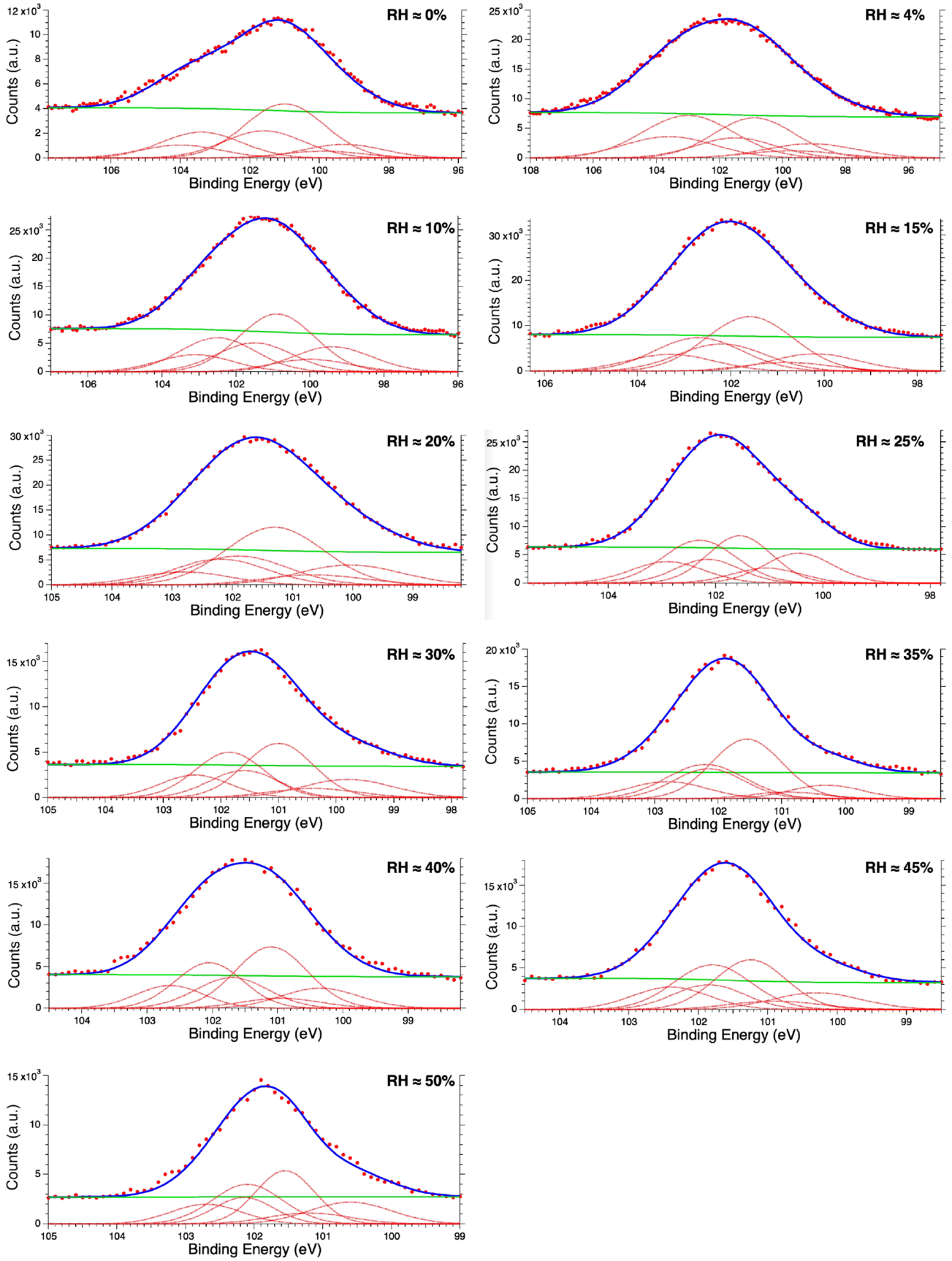

Figure 7. Si 2p NAP-XPS spectra of mica−OH-Na obtained for increasing relative humidity.

https://doi.org/10.1021/acs.jpcc.6c03757
J. Phys. Chem. C 2026, 130, 11831−11846

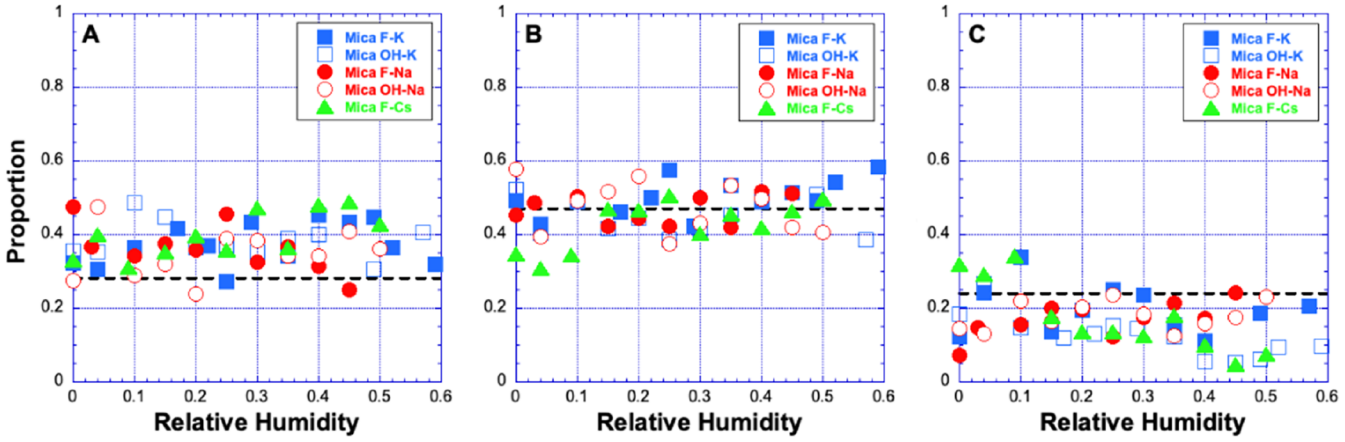

Figure 8. Evolution with relative humidity of the proportions of the various Si $2p_{3/2}$ signals for all micas. (A) High BE component. (B) Medium BE component. (C) Low BE component. The error bars were omitted for readability.

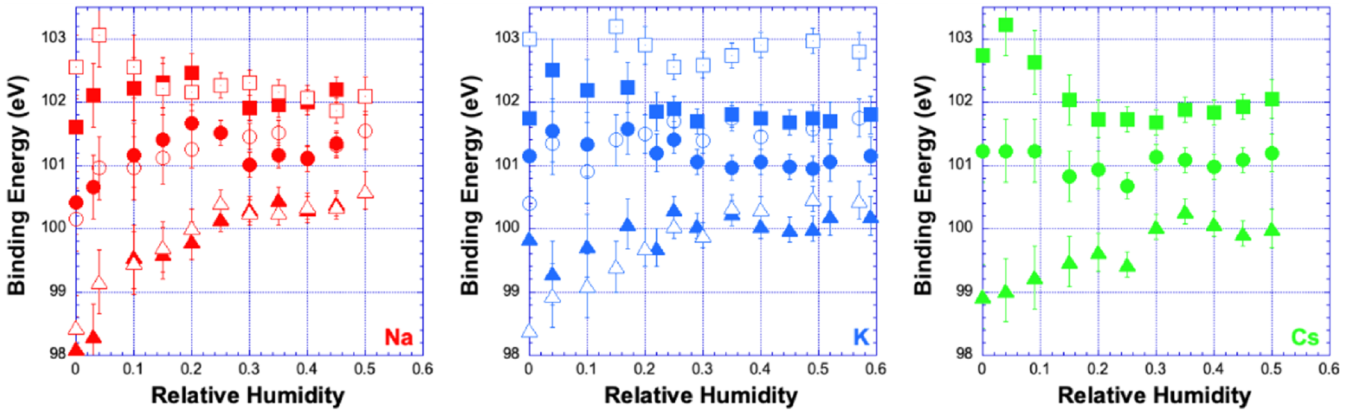

Figure 9. Evolution with relative humidity of the binding energy of the various components of the Si $2p_{3/2}$ signals. Filled symbols correspond to fluorinated micas and open ones to hydroxylated ones.

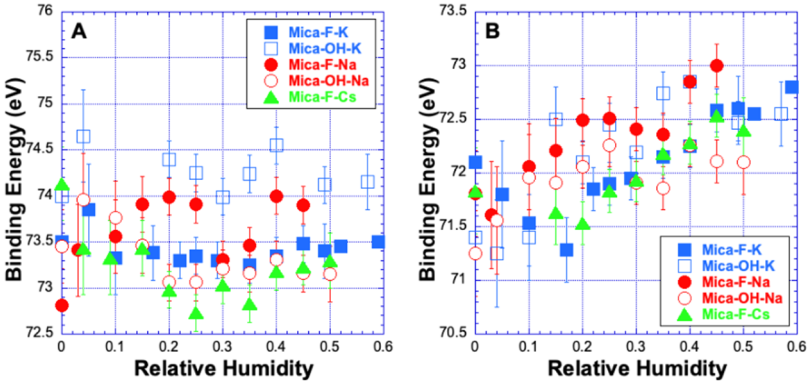

Figure 10. Evolution with relative humidity of the positions of the various Al $2p_{3/2}$ signals for all micas. (A) High BE component. (B) Low BE component.

energy component displays an increase in binding energy with increasing RH for the three cations. Such an evolution occurs mainly at low RH, i.e., for values of <0.35, and is more marked for Na^+ and relatively modest for Cs^+. In the case of K^+, the increase seems to be slightly higher for OH-mica compared to the fluorinated one. Such an evolution confirms the above-proposed assignment of the various Si signals. Indeed, the lower-energy component, being more charged due to the presence of more Al surrounding Si atoms, has more cations around it. It is then more affected by hydration than the other components. Furthermore, the comparison between the different cations follows the hydration trends deduced from the simulation results presented in Figure 4.

Aluminum. The Al 2p spectra and the associated fits obtained for increasing relative humidity are presented in Supporting Information (Figures S14−S18). The BE range of the signal is coherent with what is reported in the literature for micas,[33−35] where generally only one value is reported around 74 eV. However, in our case, the signals remain rather broad, whatever the relative humidity and nature of the sample, which

https://doi.org/10.1021/acs.jpcc.6c03757
J. Phys. Chem. C 2026, 130, 11831−11846

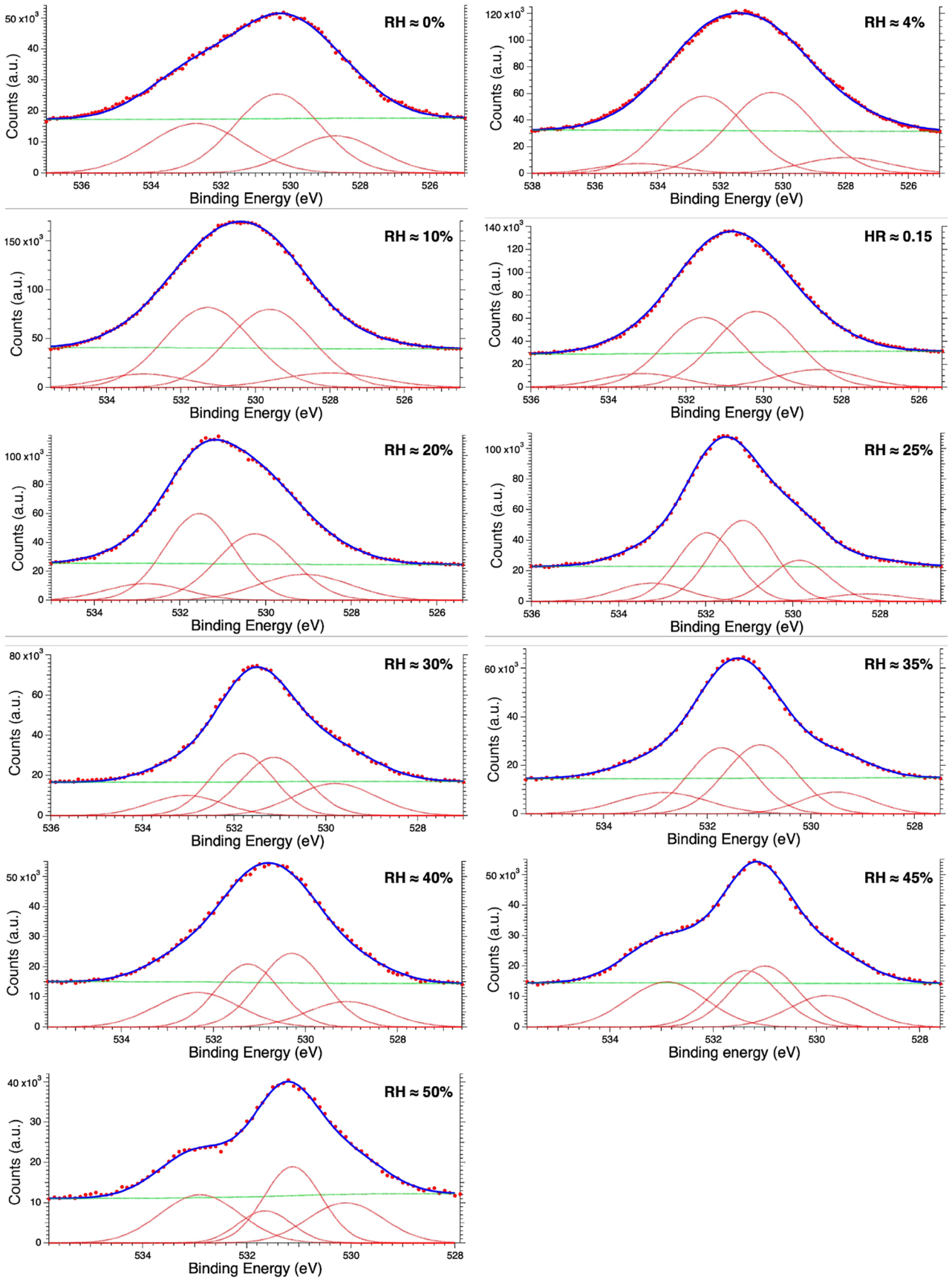

Figure 11. O 1s NAP-XPS spectra of mica−OH-Na obtained for increasing relative humidity.

https://doi.org/10.1021/acs.jpcc.6c03757
J. Phys. Chem. C 2026, 130, 11831−11846

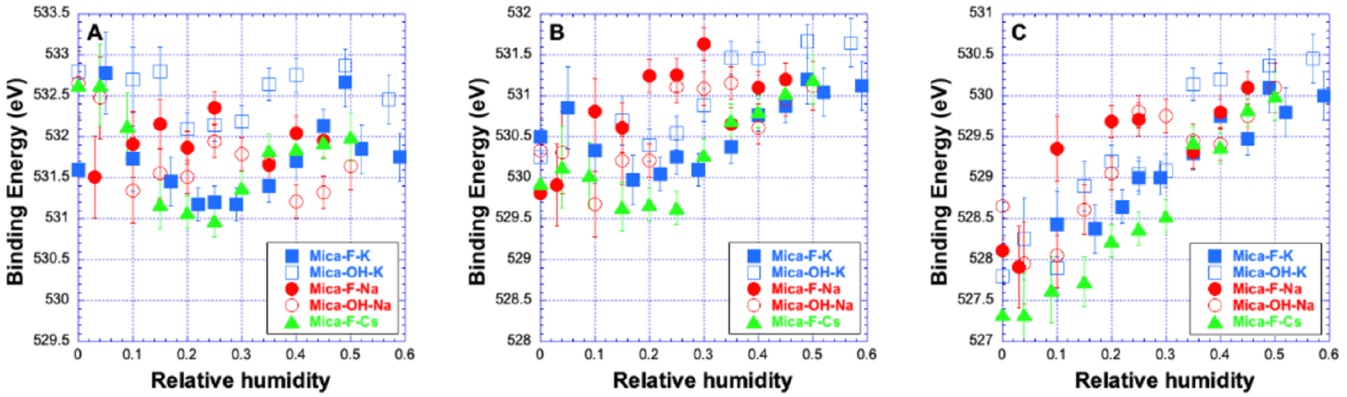

Figure 12. Evolution with relative humidity of the positions of the O 1s signals for all micas. (A) High BE component. (B) Middle BE component. (C) Low BE component.

suggests that several components must be considered in the spectra. Although Al appears to have only Si atoms as its nearest neighbors, its binding energy can vary because an Al atom located on the surface may be surrounded by 0 to 3 cations. Furthermore, all the Al atoms located deeper within the particle will be surrounded by 3 cations. In view of the low intensity of the signal, we decided to use only two components to fit the experimental spectra. The relative proportion of these two signals was found to be approximately 50%. At first glance, the low binding energy component varies monotonically with relative humidity (Figure 10), which could indicate that the Al atoms corresponding to this component are located at the surface and/or surrounded by more cations capable of hydrating, similar to the Si atoms.

Oxygen. Figure 11 displays the O 1s spectra obtained in the case of Mica−OH-Na. All spectra for other micas are presented in the Supporting Information (Figures S19−S22).

In all cases, the spectra at 0 RH can be fitted using three components located around 529.5, 530.5, and 532 eV. For higher relative pressures, an additional component located at ≈533 eV appears. The intensity of this latter signal increases significantly with relative humidity. It can then be assigned, as shown in various recent publications,[23,45,59,60,64−66] to oxygen atoms of adsorbed water, and its evolution will be described in detail in the following section. The three lower binding energy signals can in contrast be assigned to structural oxygen groups.

Figure 12 displays the evolution with RH of the position of these 3 signals assigned to structural oxygen atoms. The hydroxylated or fluorinated nature of the sample does not seem to have a significant influence on the positions of the various components. The high-energy signal (Figure 12A) does not exhibit any monotonous evolution with relative humidity. In contrast, the low-energy signal (Figure 12C) displays a clear shift of binding energy values toward higher values regardless of the sample. To a lesser extent than the low-energy signal, the energy of the intermediate signal (Figure 12B) appears to increase overall with humidity. In terms of relative proportions, even if the data are more scattered than for Al or Si, the lower binding energy component accounts for ≈20% of the signal, whereas the two higher energy ones both correspond to roughly 40% of the total oxygen peak.

In talc (uncharged clay layers with the same structure as phlogopite), O 1s position is reported around 532,5 eV.[50] In the case of micas, the binding energies of O 1s are expected to be disrupted by the presence of the Al substitutions to which surface O atoms are bonded and by the presence of cations in the adjacent trigonal cavities. There are therefore many different oxygen atoms, depending on whether they are located on the surface (bound or unbound to an Al atom and close to 0, 1, 2, or 3 cations) or within the layer, and it is not easy to assign the various peaks to them. Nevertheless, it should be noted that the component least dependent on relative humidity has a binding energy close to the O 1s value obtained in talc, which would correspond to the oxygen atoms least disturbed by the charges. The two components with the lowest energies would then correspond to O atoms whose electronic environment is disturbed by the presence of charges (Al substitution or cations) and which are the most sensitive to cation hydration. It can be observed that, overall, Na-micas exhibit an increase in their binding energy at lower relative humidity levels than those of K-micas and Cs-micas, which is consistent with the hydration of cations as observed in simulations and described earlier.

The highest energy signal whose area increases with RH can be assigned to hydration water, and its evolution is therefore directly linked to surface hydration. Except for some samples at very low RH, where charge effects are maximal, the position of this signal is almost constant around 533 eV, and no significant differences between fluorinated and hydroxylated micas can be observed. The relative proportion displayed in Figure 13 represents the ratio between the area of the peak assigned to hydration water and the sum of the areas of the peak assigned to the structural oxygens of micas.

The evolution of its relative area (Figure 13) with an increase in RH can be considered as a water adsorption isotherm. Since OH-mica contains 1.2 times more structural oxygens per unit cell than F-mica, it is expected that for the same amount of water adsorbed onto the surface, the proportion of the peak assigned to water will be greater in the case of F-mica than in that of OH-mica by a factor of 1.2. As a consequence, the relative proportions obtained for mica-F were therefore divided by 1.2 so that they could be compared to those of mica−OH.

Figure 13 reveals significant features. First of all, it is clear that fluorinated samples display significantly less water adsorption than their hydroxylated counterparts, at least at low humidities. As regards mica-F, it is generally observed that the isotherm for mica−F-Na lies above that for mica−F-K, which lies above that of mica−F-Cs, with the exception of a few isolated points. As regards mica−OH, the isotherms for mica−OH-Na and mica-OH-K are quite similar except for very

https://doi.org/10.1021/acs.jpcc.6c03757
J. Phys. Chem. C 2026, 130, 11831−11846

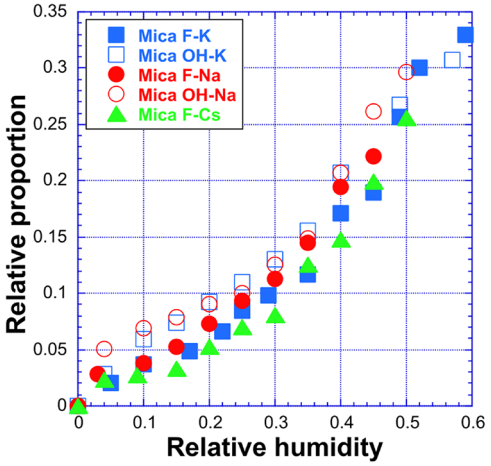

Figure 13. Evolution with relative humidity of the relative proportion of the O 1s signal corresponding to hydration water. The error bars were omitted for readability.

low humidity levels, where the isotherm for mica−OH-Na lies clearly above that for mica−OH-K.

It is worth examining the simulation results to check whether they reproduce the trends observed in the sample's hydration and whether they can help explain the experimental results observed. Table 1 summarizes the calculated ΔF_{dry} and ΔF_{wet} per cation, and the resulting ΔF for all of the samples of interest.

First, the values of ΔF_{wet} can be compared to those obtained by Bourg et al.[22] for muscovite micas. In our case, the investigated mica is phlogopite. The only difference between the two species lies in the composition of the octahedral layer, which is made of Al for muscovite, vs Mg for phlogopite. Using data reported in Figure 7 of this article,[22] reported values for ΔF_{wet} for (Mica−OH-Cs → Mica−OH-K) and for (Mica−OH-Cs → Mica−OH-Na) are −45 and −108 kJ/mol per cation, whereas our values for the same transformation are −40 and −137 kJ/mol per cation (Table 1). The values are in good agreement for the transformation Cs → K, and are more different for Cs → Na. The small discrepancies in the Cs → K case could be assigned to the different nature of the mica or to the fact that, in our work, we allowed relaxation of ditrigonal cavities, which minimizes cavity distortion compared with the case of rigid layers examined in ref 22 The stronger discrepancy observed in the Cs → Na can be due to the choice of the Lennard-Jones parameters for Na^+. Indeed, in the present work, the parameters provided by Smith and Dang were chosen,[67] whereas the parameters proposed by Dang[68] were implemented in ref 22.

Data in Table 1 can be used to classify the micas used in the present study from the most hydrophobic to the most hydrophilic. The following order is then obtained: Mica−F-K, Mica−F-Na, Mica−F-Cs, Mica−OH-K, Mica−OH-Cs, Mica−OH-Na. Taking the most hydrophobic mica (Mica−F-K) as a reference, ΔW, the difference in work of adhesion between other micas and this reference sample can be calculated. This yields ΔW = 5.8, 11.1, 15.8, 20.5, and 43.4 kJ/mol of cations for Mica−F-Na, Mica−F-Cs, Mica−OH-K, Mica−OH-Cs, and Mica−OH-Na, respectively. It can be noted that, according to this list, fluorinated micas are more hydrophobic than hydroxylated ones. Such a result qualitatively agrees with experimental/simulation results obtained with fluorinated smectite clays that show that fluorinated swelling clays are more hydrophobic than hydroxylated ones.[46−48,54,69,70] This also concurs with experimental NAP-XPS results (Figure 13), as water adsorption in this humidity range is higher for hydroxylated micas than for fluorinated ones.

Two additional facts can be deduced from this Table. (i) Mica−OH-Na is by far the most hydrophilic of the investigated samples. This appears logical, as, among the 3 studied cations, Na^+ has the highest hydration energy. This can be related to water adsorption experiments on smectite clays exchanged with monovalent cations.[71] However, this is not the case for the fluorinated mica, which appears more hydrophilic with Cs^+ than with Na^+. (ii) The presence of K^+ leads to an increased hydrophobicity of mica−OH, compared to other cations. This concurs with the fact that K^+ ions are considered as swelling inhibitors,[72] but is not in line with the hydration energy of K^+, which is higher than that of Cs^+. Still, it is known that K^+ fits perfectly in the ditrigonal cavity of micas, which increases the affinity of this ion for the surface. This strong affinity was shown in the Raman analysis of water adsorption on K-exchanged saponite[73] and in a recent simulation work[74] that reveals, using ab initio calculations, that the desorption barrier for removing K^+ from a muscovite surface is very high. To reinforce our confidence in simulation results and as a sensitivity test, in the case of OH-micas exchanged with various monovalent cations, we decided to calculate ΔW again by modifying certain characteristics of the surface. We then used a mica surface equilibrated using the polarizable force field PIM, which is known to yield more realistic fine unit cell characteristics.[75,76] This is particularly the case regarding the deformation of ditrigonal cavities. This could play a role in cation adsorption at the surface, especially in the dry state, which could then affect the initial hydration states. Positions of the clay atoms were fixed during the simulations in order to prevent the relaxation of the clay sheets. The works of adhesion were calculated only for the most hydrated systems. Wettability differences between the various micas were found to be less important than when relaxed surfaces were used. Still, the hydrophobicity scale deduced from these simulations remained unchanged, i.e., mica−OH-K was the most hydrophobic and mica−OH-Na the most hydrophilic. $\Delta W = W -$

Table 1. Energetic Quantities of the Thermodynamic Cycle of Figure 1 for Several Alchemical Transformations; the Units Are kJ/mol of Cations; Errors Are Smaller than the Precision of the Numbers (< 0.05 kJ/mol of Cations)

	ΔF_{dry}(kJ/mol C^+)	ΔF_{wet}	$\Delta W = W_2 - W_1$
Mica−OH-Cs → Mica−OH-K	−44.3	−39.6	−4.7
Mica−OH-Cs → Mica−OH-Na	−114.1	−136.9	22.8
Mica−OH-Cs → Mica−F-Cs	393.5	403.0	−9.4
Mica−OH-K → Mica−F-K	383.4	399.2	−15.8
Mica−OH-Na → Mica−F-Na	372.0	409.6	−37.6

https://doi.org/10.1021/acs.jpcc.6c03757
J. Phys. Chem. C 2026, 130, 11831−11846

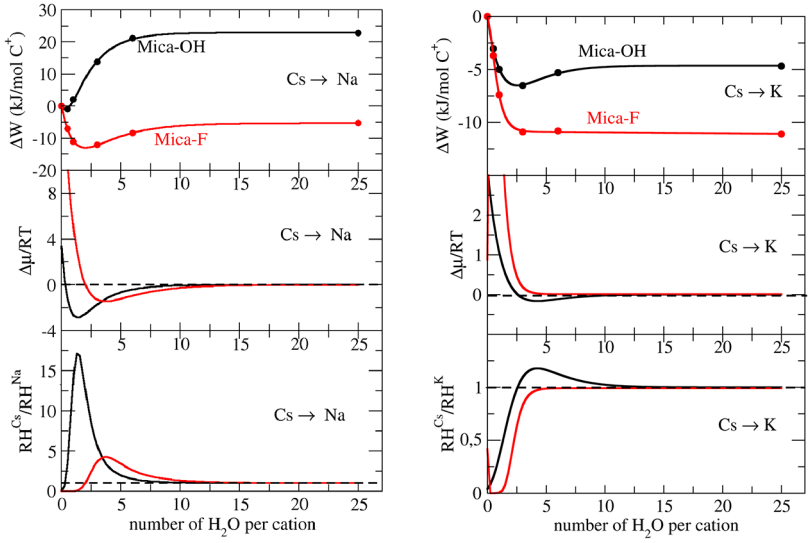

Figure 14. Simulated $\Delta W(N)$ for various numbers of H_2O per cation adsorbed on the surfaces of micas (circle symbols). Black: Mica−OH, red: Mica-F. Left: Alchemical transformation Cs → Na; right: alchemical transformation Cs → K. Simulation points were interpolated by a function that was then derived to measure $\Delta\mu(N)$ and RH_2/RH_1.

$W(K)$ values of 4.3 and 18.4 kJ/mol of cation were obtained for mica−OH-Cs and mica−OH-Na, respectively. The corresponding values obtained using the first procedure and relaxed ditrigonal cavities were 4.7 and 27.6 kJ/mol of cation. The lower values obtained reveal a weaker interaction between cations and the surface, which is further illustrated by comparing the radial distribution functions obtained in both cases for Cs and Na (Figure S23). It reveals significantly less structuring in the case of deformed cavities compared to the case where ditrigonal cavities are relaxed. Still, independently of the model chosen for the surface, it appears that the hydrophobicity scale deduced from our simulations remains valid.

To go further in our analysis, we analyzed ΔW in more detail. Assimilating the free energy to the free enthalpy, and considering that the average number of water molecules adsorbed on the surface is roughly equal to the initial number of water molecules put in the box (the number of water molecules leaving the adsorbed layer for the vapor phase during a simulation run being very low), ΔW can also be interpreted as the difference between the free enthalpies of adsorption of the water layer, i.e., $\Delta W = -\int_0^N \Delta\mu(N)\, dN$, where $\Delta\mu(N) = \mu_2(N) - \mu_1(N)$ is the difference of chemical potential of adsorbed water between system 2 and system 1 when N water molecules are adsorbed. $\Delta\mu(N) = RT \ln \frac{RH_2}{RH_1}$ is directly linked to the ratio between the relative humidities of system 2 and system 1 for which the same number of water molecules N is adsorbed on the surface. For a given quantity of adsorbed water N, $RH_2 < RH_1$ indicates that system 2 adsorbs N water molecules at a lower relative humidity than system 1. Consequently, system 2 can be viewed as more hydrophilic than system 1 for this N value, and the term $\Delta\mu(N)$ that is negative in this case, contributes negatively to the integral. The difference of work of adhesion ΔW is the sum of all of these terms, which can take different signs between 0 and 100% of humidity. ΔW can then be calculated if the full water adsorption isotherm is known. This is not the case with our NAP/XPS experiments that are limited to RH ≤ 60%. This was not the case either in other studies,[23] where the low RH range could not be analyzed. To better understand the role of the first hydration states of mica on wetting properties, simulations were then undertaken to calculate ΔW at hydration states corresponding to humidities lower than 100%. The alchemical transformations of Figure 1 were carried out for mica surfaces in hydration states corresponding to 0.5, 1, 3, and 6 H_2O per cation. Considering, as in Koishi et al.,[23] that one monolayer of water corresponds to 5.25 H_2O per unit cell (therefore 5.25 H_2O per cation), the chosen values correspond roughly to 0.1, 0.2, 0.5, 1, and 5 monolayers. After plotting $\Delta W(N)$ as a function of N, the obtained curve was interpolated. The derivation of this interpolated curve yielded $\Delta\mu(N) = RT \ln \frac{RH_2}{RH_1}$ as well as the ratio RH_2/RH_1.

Figure 14 displays the results of applying such a procedure. Let us first consider the results obtained for the alchemical transformations of Cs to Na (left panel of Figure 14). In the case of mica−OH (black curve), it appears that except for very low relative humidities, $\Delta W(N) = W_{Na} - W_{Cs}$ is always positive and the ratio RH_{Cs}/RH_{Na} is significantly higher than 1. This shows that the surface with Na^+ is always more hydrophilic than that with Cs^+. Unfortunately, the NAP/XPS isotherm for Mica−OH-Cs could not be measured, which precludes a direct comparison between experiment and simulation. For mica-F (red curves in Figure 14), the Cs^+ sample appears more hydrophilic at low hydration states (<≈0.5 monolayer of water adsorbed), whereas the contrary is observed for higher adsorbed amounts, for which RH_{Cs}/RH_{Na} is higher than 1. At low surface coverage, the cesium surface could be more hydrophilic than the sodium one, due to interactions between fluorine and small Na^+ cations that could be stronger than with Cs^+. For higher adsorbed water amounts, mica−F-Na becomes more hydrophilic than mica−F-Cs as RH_{Cs}/RH_{Na} is higher than 1.

The comparison with experiments (Figure 13) reveals a good agreement at high RH and a minor discrepancy at low RH. Indeed, considering that the adsorption of a 0.5 water monolayer occurs for RH values of ≈10%,[23,26] experimental NAP/XPS results do not fully agree with simulations, as for the first point at low RH, the Na sample adsorbs more water,

https://doi.org/10.1021/acs.jpcc.6c03757
J. Phys. Chem. C 2026, 130, 11831−11846

whereas simulations predict a $RH_{Cs}/RH_{Na} < 1$. Given the precision of experiments in the low RH range where charge effects are important, this small discrepancy can be considered as not significant.

At this stage, it should be pointed out that these calculations show that the hydrophilic or hydrophobic character of a surface largely depends on the first stages of surface hydration: even if RH_{Cs}/RH_{Na} is higher than 1 on most of the adsorption isotherms (RH > ≈10%, Figure 14, red curve), it cannot be concluded that mica−F-Na is overall more hydrophilic than mica−F-Cs. Based on Table 1, it even appears as the opposite: this demonstrates the importance of the very early stages of surface wetting on wettability properties.

To better understand the significant difference in behavior between hydroxylated and fluorinated mica, it is relevant to closely explore the cation environment. In that regard, the structure of surfaces in the dry state is quite revealing: in most configurations and regardless of the compensating cation, the cations are located above the ditrigonal cavities surrounded by the six oxygen atoms of the cavities. However, in the case of mica−OH-Na, some cations are located above a silicon atom bonded to only three oxygen atoms (see Figure S2), which shows that the position above the cavities is not necessarily the most favorable. In comparison, for mica−F-Na, such a location does not exist. The existence of such sites that could facilitate cation hydration could explain the high hydrophilicity of mica−OH-Na. Further insight can be obtained by plotting the radial distribution functions Na-OS (Figure S3). As has already been mentioned above, in the case of mica−F-Na, $g(r)$ in the dry state and for 1 H_2O per cation are almost superimposed. In contrast, for mica−OH-Na, significant differences between both curves can be observed, with notably a shift of the first peak of $g(r)$ to higher distances when water is added, which reveals that Na^+ ions in this mica move away from the solid surface as soon as small amounts of water are adsorbed. This again points toward a high hydrophilicity of Mica−OH-Na. In terms of comparison with experiments, a very good agreement is obtained at low RH (<0.2), where mica−OH-Na adsorbs significantly more water than its fluorinated counterpart.

Let us now consider the alchemical transformations of Cs to K displayed in the right-hand panel of Figure 14. For mica−F-K, simulations reveal that RH_{Cs}/RH_K is lower than 1 at low hydration and roughly equal to 1 for higher water-adsorbed amounts. This suggests that both isotherms should be very similar except at very low RH, where that of mica−F-Cs should be above that of mica−F-K. Looking at the data in Figure 13, it appears that both isotherms are very close to each other except for some isolated points (around RH = 0.3 and RH = 0.4) where mica−F-K seems to absorb more water than mica−F-Cs. Considering the precision of the analysis of O 1s spectra, the agreement between experiment and simulations is rather satisfactory in this case.

Finally, Figure S24 presents the simulated results comparing mica−OH-K and mica−OH-Na. It appears that at low RH, mica−OH-Na is significantly more hydrophilic, whereas at higher RH (roughly for a bilayer of water), both samples appear to behave similarly. This concurs with experimental results (Figure 13) as, at low RH, mica−OH-Na adsorbs more water than mica−OH-K, whereas for high RH, considering the possible uncertainties in fitting, both samples behave similarly.

Considering the uncertainty in the analysis of experiments at low RH where charge effects are important and where the signal corresponding to adsorbed water is rather weak, as well as the difficulties associated with simulations that are sensitive to both the fine structure of the surface and the choice of the force field, the agreement obtained here between experiments and simulations is really satisfactory. In particular, in the whole low RH range that is crucial in the wetting phenomenon, qualitative agreement between NAP-XPS experiments and molecular simulations is reached, which illustrates the potential of this approach to understand the fine details of wetting of mineral surfaces.

CONCLUSION

In this article, near-ambient-pressure XPS measurements of the early hydration stages of phlogopite mica, combined with molecular simulations, were presented. The roles of both surface-bound monovalent cations and the replacement of structural hydroxyl groups by fluorine atoms were investigated. The environments of the atoms constituting the system (structural atoms, counterions, and water molecules) were studied as a function of the relative humidity. It has been shown that the various contributions to the XPS spectrum for surface Si and Al atoms depend on the surface hydration state and the amount of cations in the vicinity: the differences in binding energy between these components tend to decrease with relative humidity, particularly as the cations readily hydrate and move away from the surface, as shown by the simulations.

The evolution of the NAP-XPS component of O, attributed to hydration water with relative humidity (RH), was considered as representative of a water adsorption isotherm. At low RH (≤0.2), fluorinated samples show significantly lower water adsorption than their hydroxylated counterparts. This is consistent with the behavior of the NAP-XPS components of the counterions that revealed a delay in hydration for the fluorinated sample compared to the hydroxylated sample, particularly in the case of Na^+. In order to perform a quantitative comparison with NAP/XPS experiments and to further interpret the adsorption isotherms, alchemical transformations at different surface water contents were performed using molecular dynamics. This allowed calculating for two different micas the ratio between relative humidities for a given surface water amount. In the case of mica−OH, simulations showed that the surface with Na^+ is always more hydrophilic than that with Cs^+. For mica-F, the Cs^+ sample appears to be more hydrophilic at low hydration states (≤≈0.5 monolayer of adsorbed water), while the opposite is observed for higher amounts of adsorbed water. It may be that at low surface coverages, the interactions between fluorine and small Na^+ cations are stronger than with Cs^+. Despite the uncertainties associated with both the NAP-XPS experiment and the force field used in simulations, the comparison between experiments and simulations yields good agreement at high relative humidity and minor discrepancies at low relative humidity. It should be noted that simulations show that the hydrophilic or hydrophobic nature of a surface largely depends on the early stages of surface hydration. Indeed, simulations reveal that even though most of the adsorption isotherm seems to suggest that mica−F-Cs is more hydrophobic than mica−F-Na, the opposite is actually true: the adhesion work calculated using the same alchemical method on well-hydrated samples (corresponding to ≈ 100% RH) ranks increasing hydrophilicity in the following order: F−K mica, F−Na mica, F−Cs mica, OH-K mica, OH-Cs mica, OH-Na mica. The hydrophilic/hydrophobic nature of the surface

https://doi.org/10.1021/acs.jpcc.6c03757
J. Phys. Chem. C 2026, 130, 11831−11846

strongly depends on the very first hydration stages, i.e., on the balance between cation/surface and cation/water interactions. Consequently, experiments aiming at assessing hydrophobicity must be able to analyze the initial hydration stages. In that regard, the NAP/XPS technique appears particularly powerful, as low relative humidities can be studied. Still, it must be pointed out that, in that region, charge effects are important, which requires an efficient procedure for correcting them. The original simulation approach based on thermodynamic integration that we used in the present work does not allow direct measurement of adsorption isotherms, unlike Grand Canonical Monte Carlo methods or others.[23,74,77,78] However, such a technique is very insensitive to statistical problems and therefore offers optimal accuracy, which makes it an ideal complement to more classical simulation techniques. In view of the relevance of the comparison between NAP-XPS and molecular simulations evidenced by the present study, an obvious continuation of this work would be to extend the investigated systems by examining the influence of divalent (alkaline earth metals) and trivalent (La^{3+}) cations. In that case, cation hydration energies will be higher, whereas fewer cations will be present at the surface. The combination of these two features should have a significant impact on hydration and the environment of surface atoms. However, it should be noted that in that case, using a polarizable force field such as PIM[54,79] may well be essential.

■ ASSOCIATED CONTENT

Supporting Information

The Supporting Information is available free of charge at https://pubs.acs.org/doi/10.1021/acs.jpcc.6c03757.

Snapshot of a simulation box of hydroxylated phlogopite with Na^+, containing 25 H_2O per cation; starting and final configurations of the alchemical transformation of OH in F for mica-Na; radial distribution functions between Na and Os for dry Na exchanged micas and Na exchanged micas hydrated with 1 H_2O per cation; evolution with relative humidity of Cs 3d signals of Mica−F-Cs, K 2p signals of Mica−OH-Na, K 2p signals of Mica−OH-K, K 2p signals of Mica−F-Na, K 2p signals of Mica−F-K, K 2p signals of Mica−F-Cs, Si 2p signals of Mica−OH-K, Si 2p signals of Mica−F-Na, Si 2p signals of Mica−F-K, Si 2p signals of Mica−F-Cs, Al 2p signals of Mica−OH-Na, Al 2p signals of Mica−OH-K, Al 2p signals of Mica−F-Na, Al 2p signals of Mica−F-K, Al 2p signals of Mica−F-Cs, O 2s signals of Mica−OH-K, O 2s signals of Mica−F-Na, O 2s signals of Mica−F-K, O 2s signals of Mica−F-Cs; radial distribution functions between cation and Os for dry hydroxylated micas with deformed cavities obtained with PIM force field and with relaxed cavities; and simulated ratio of relative humidities of Mica−OH-K and Mica−OH-Na as a function of the number of H_2O per cation adsorbed on the surface (PDF)

■ AUTHOR INFORMATION

Corresponding Author

Virginie Marry − *Physicochimie des Electrolytes et des Nanosystèmes InterfaciauX (Phenix) UMR 8234, CNRS-Sorbonne Université, 75005 Paris, France;* orcid.org/0000-0001-5743-4844; Email: virginie.marry@sorbonne-universite.fr

Authors

Laurent J. Michot − *Physicochimie des Electrolytes et des Nanosystèmes InterfaciauX (Phenix) UMR 8234, CNRS-Sorbonne Université, 75005 Paris, France*

Loïc Guérin − *Physicochimie des Electrolytes et des Nanosystèmes InterfaciauX (Phenix) UMR 8234, CNRS-Sorbonne Université, 75005 Paris, France*

Théophane Bernhard − *Physicochimie des Electrolytes et des Nanosystèmes InterfaciauX (Phenix) UMR 8234, CNRS-Sorbonne Université, 75005 Paris, France*

Ayumi Koishi − *Institut des Sciences de la Terre Université Grenoble Alpes (ISTerre) UMR 5275, 38058 Grenoble, France; RIKEN Center for Sustainable Resource Science, Biofunctional Catalyst Research Team, Wako, Saitama 351-0198, Japan;* orcid.org/0000-0002-6185-8241

Francis Claret − *Bureau de Recherches Géologiques et Minières (BRGM), 45060 Orléans, France*

Eric Ferrage − *Hydrasa - Institut de chimie des milieux et matériaux de Poitiers (IC2MP) UMR 7285, 86073 Poitiers, France*

Jean-Jacques Gallet − *Laboratoire de Chimie Physique-Matière et Rayonnement (LCPMR) UMR 7614, CNRS-Sorbonne Université, 75005 Paris, France;* orcid.org/0000-0003-2076-1432

Fabrice Bournel − *Laboratoire de Chimie Physique-Matière et Rayonnement (LCPMR) UMR 7614, CNRS-Sorbonne Université, 75005 Paris, France*

Complete contact information is available at: https://pubs.acs.org/10.1021/acs.jpcc.6c03757

Notes

The authors declare no competing financial interest.

■ ACKNOWLEDGMENTS

The authors are grateful to the CNRS interdisciplinary "défi Needs" program (Project DARIUS) for funding. The authors acknowledge synchrotron SOLEIL for granting them beamtime on the TEMPO beamline. The experimental help of Marina Descoubes and Félicien Pauly during the NAP-XPS experiments is gratefully acknowledged.

■ REFERENCES

(1) Chong, S.-H.; Ham, S. Distinct Role of Hydration Water in Protein Misfolding and Aggregation Revealed by Fluctuating Thermodynamics Analysis. *Acc. Chem. Res.* **2015**, *48*, 956−965.

(2) Monroe, J.; Barry, M.; De Stefano, A.; Gokturk, P.; Jiao, S.; Robinson-Brown, D.; Webber, T.; Crumlin, E.; Han, S.; Shell, M. Water Structure and Properties at Hydrophilic and Hydrophobic Surfaces. *Annu. Rev. Chem. Biomol. Engng.* **2020**, *11*, 523−557.

(3) Jaegers, N. R.; Wang, Y.; Hu, J.; Wachs, I. Impact of Hydration on Supported V2O5/TiO2 Catalysts as Explored by Magnetic Resonance Spectroscopy. *J. Phys. Chem. C* **2021**, *125*, 16766−16775.

(4) Huang, J.; Lin, C.; Tanaka, Y.; Yamamoto, A.; Luo, S.; Tanaka, M. Manipulation of Surface Hydration States by Tuning the Oligo(Ethylene Glycol) Moieties on PEDOT to Achieve Platelet-Resistant Bioelectrode Applications. *Adv. Mater. Interf* **2022**, *9*, No. 2200707.

(5) Qian, Y.; Deng, G.; Lapp, J.; Rao, Y. Interfaces of Gas-Aerosol Particles: Relative Humidity and Salt Concentration Effects. *J. Phys. Chem. A* **2019**, *123*, 6304−6312.

(6) Ge, P.; Luo, G.; Luo, Y.; Huang, W.; Xie, H.; Chen, J.; Qu, J. Molecular understanding of the interaction of amino acids with sulfuric acid in the presence of water and the atmospheric implication. *Chemosphere* **2018**, *210*, 215−223.

(7) National Research Council. *Basic Research Opportunities in Earth Science*; National Academies Press: Washington, DC, 2001.
(8) Michot, L. J.; Villiéras, F.; François, M.; Bihannic, I.; Pelletier, M.; Cases, J.-M. Water Organisation at the Solid-Aqueous Solution Interface. *C. R. Geosci.* **2002**, *334*, 611−631.
(9) Ferrage, E.; Sakharov, B. A.; Michot, L. J.; Delville, A.; Bauer, A.; Lanson, B.; Grangeon, S.; Frapper, G.; Jiménez-Ruiz, M.; Cuello, G. J. Hydration Properties and Interlayer Organization of Water and Ions in Synthetic Na-Smectite with Tetrahedral Layer Charge. Part 2. Toward a Precise Coupling between Molecular Simulations and Diffraction Data. *J. Phys. Chem. C* **2011**, *115*, 1867−1881.
(10) Marry, V.; Dubois, E.; Malikova, N.; Durand-Vidal, S.; Longeville, S.; Breu, J. Water Dynamics in Hectorite Clays: Influence of Temperature Studied by Coupling Neutron Spin Echo and Molecular Dynamics. *Environ. Sci. Technol.* **2011**, *45*, 2850−2855.
(11) Michot, L. J.; Ferrage, E.; Jiménez-Ruiz, M.; Boehm, M.; Delville, A. Anisotropic Features of Water and Ion Dynamics in Synthetic Na- and Ca-Smectites with Tetrahedral Layer Charge. A Combined Quasi-Elastic Neutron-Scattering and Molecular Dynamics Simulations Study. *J. Phys. Chem. C* **2012**, *116*, 16619−16633.
(12) Marry, V.; Dubois, E.; Malikova, N.; Breu, J.; Haussler, W. Anisotropy of Water Dynamics in Clays: Insights from Molecular Simulations for Experimental QENS Analysis. *J. Phys. Chem. C* **2013**, *117*, 15106−15115.
(13) Dazas, B.; Lanson, B.; Delville, A.; Robert, J.-L.; Komarneni, S.; Michot, L. J.; Ferrage, E. Influence of Tetrahedral Layer Charge on the Organization of Interlayer Water and Ions in Synthetic Na-Saturated Smectites. *J. Phys. Chem. C* **2015**, *119*, 4158−4172.
(14) Jiménez-Ruiz, M.; Ferrage, E.; Blanchard, M.; Fernández-Castañon, J.; Delville, A.; Johnson, M. R.; Michot, L. J. Combination of Inelastic Neutron Scattering Experiments and ab Initio Quantum Calculations for the Study of the Hydration Properties of Oriented Saponites. *J. Phys. Chem. C* **2017**, *121*, 5029−5040.
(15) Petersen, M. H.; Vernet, N.; Gates, W. P.; Villacorta, F. J.; Ohira-Kawamura, S.; Kawakita, Y.; Arai, M.; Kneller, G. R.; Bordallo, H. N. Assessing Diffusion Relaxation of Interlayer Water in Clay Minerals Using a Minimalist Three-Parameter Model. *J. Phys. Chem. C* **2021**, *125*, 15085−15093.
(16) Pashley, R. M. Hydration Forces between Mica Surfaces in Electrolyte Solutions. *Adv. Colloid Interface Sci.* **1982**, *16*, 57−62.
(17) Pashley, R. M.; Quirk, J. P. The Effect of Cation Valency on DLVO and Hydration Forces between Macroscopic Sheets of Muscovite Mica in Relation to Clay Swelling. *Colloids Surf.* **1984**, *9*, 1−17.
(18) Rotsch, C.; Radmacher, M. Mapping Local Electrostatic Forces with the Atomic Force Microscope. *Langmuir* **1997**, *13*, 2825−2832.
(19) Kobayashi, K.; Oyabu, N.; Kimura, K.; Ido, S.; Suzuki, K.; Imai, T.; Tagami, K.; Tsukada, M.; Yamada, H. Visualization of Hydration Layers on Muscovite Mica in Aqueous Solution by Frequency-Modulation Atomic Force Microscopy. *J. Chem. Phys.* **2013**, *138*, No. 184704.
(20) Park, C.; Fenter, P. A.; Nagy, K. L.; Sturchio, N. C. Hydration and Distribution of Ions at the Mica-Water Interface. *Phys. Rev. Lett.* **2006**, *97*, No. 016101.
(21) Schlegel, M. L.; Nagy, K. L.; Fenter, P.; Cheng, L.; Sturchio, N. C.; Jacobsen, S. D. Cation Sorption on the Muscovite (001) Surface in Chloride Solutions Using High-Resolution X-Ray Reflectivity. *Geochim. Cosmochim. Acta* **2006**, *70*, 3549−3565.
(22) Bourg, I. C.; Lee, S. S.; Fenter, P.; Tournassat, C. Stern Layer Structure and Energetics at Mica-Water Interfaces. *J. Phys. Chem. C* **2017**, *121*, 9402−9412.
(23) Koishi, A.; Lee, S. S.; Fenter, P.; Fernandez-Martinez, A.; Bourg, I. C. Water Adsorption on Mica Surfaces with Hydrophilicity Tuned by Counterion Types (Na, K, and Cs) and Structural Fluorination. *J. Phys. Chem. C* **2022**, *126*, 16447−16460.
(24) Zhao, G.; Tan, Q.; Xiang, L.; Cai, D.; Zeng, H.; Yi, H.; Ni, Z.; Chen, Y. Structure and Properties of Water Film Adsorbed on Mica Surfaces. *J. Chem. Phys.* **2015**, *143*, No. 104705.
(25) Arai, T.; Sato, K.; Iida, A.; Tomitori, M. Quasi-Stabilized Hydration Layers on Muscovite Mica under a Thin Water Film Grown from Humid Air. *Sci. Rep.* **2017**, *7*, No. 4054.
(26) Balmer, T. E.; Christenson, H. K.; Spencer, N. D.; Heuberger, M. The Effect of Surface Ions on Water Adsorption to Mica. *Langmuir* **2008**, *24*, 1566−1569.
(27) Park, S. H.; Sposito, G. Structure of Water Adsorbed on a Mica Surface. *Phys. Rev. Lett.* **2002**, *89*, No. 085501.
(28) Wang, J.; Kalinichev, A. G.; Kirkpatrick, R. J.; Cygan, R. T. Structure, Energetics, and Dynamics of Water Adsorbed on the Muscovite (001) Surface: A Molecular Dynamics Simulation. *J. Phys. Chem. B* **2005**, *109*, 15893−15905.
(29) Sakuma, H.; Kawamura, K. Structure and Dynamics of Water on Li^+-, Na.-, K^+-, Cs^+-, H_3O^+-Exchanged Muscovite Surfaces: A Molecular Dynamics Study. *Geochim. Cosmochim. Acta* **2011**, *75*, 63−81.
(30) Ou, X.; Wang, X.; Lin, Z.; Li, J. Heterogeneous Condensation of Water on the Mica (001) Surface: A Molecular Dynamics Simulation Work. *J. Phys. Chem. C* **2017**, *121*, 6813−6819.
(31) Adapa, S.; Swamy, D. R.; Kancharla, S.; Pradhan, S.; Malani, A. Role of Mono− and Divalent Surface Cations on the Structure and Adsorption Behavior of Water on Mica Surface. *Langmuir* **2018**, *34*, 14472−14488.
(32) Wagner, C. D.; Passoja, D. E.; Hillery, H. F.; Kinisky, T. G.; Six, H. A.; Jansen, W. T.; Taylor, J. A. Auger and Photoelectron Line Energy Relationships in Aluminum-Oxygen and Silicon-Oxygen Compounds. *J. Vac. Sci. Technol.* **1982**, *21*, 933−944.
(33) Bhattacharyya, K. G. XPS Study of Mica Surfaces. *J. Electron Spectrosc. Relat. Phenom.* **1993**, *63*, 289−306.
(34) González-Elipe, A. R.; Espinosa, J. P.; Munuera, G.; Sanz, J.; Serratosa, J. M. Bonding-State Characterization of Constituent Elements in Phyllosilicate Minerals by XPS and NMR. *J. Phys. Chem. A* **1988**, *92*, 3471−3476.
(35) Ebina, T.; Iwasaki, T.; Chatterjee, A.; Katagiri, M.; Stucky, G. D. Comparative Study of XPS and DFT with Reference to the Distributions of Al in Tetrahedral and Octahedral Sheets of Phyllosilicates. *J. Phys. Chem. B* **1997**, *101*, 1125−1129.
(36) Okada, K.; Kameshima, Y.; Yasumori, A. Chemical Shifts of Silicon X-ray Photoelectron Spectra by Polymerization Structures of Silicates. *J. Am. Ceram. Soc.* **1998**, *81*, 1970−1972.
(37) Franceschi, G.; Brandstetter, S.; Balajka, J.; Sokolovic, I.; Pavelec, J.; Setvín, M.; Schmid, M.; Diebold, U. Interaction of Surface Cations of Cleaved Mica with Water in Vapor and Liquid Forms. *Faraday Discuss.* **2024**, *249*, 84−97.
(38) Ogletree, D. F.; Bluhm, H.; Lebedev, G.; Fadley, C. S.; Hussain, Z.; Salmeron, M. Differentially Pumped Electrostatic Lens System for Photoemission Studies in the Millibar Range. *Rev. Sci. Instrum.* **2002**, *73*, 3872−3877.
(39) Bluhm, H. Photoelectron Spectroscopy of Surfaces under Humid Conditions. *J. Electron Spectrosc. Relat. Phenom.* **2010**, *177*, 71−84.
(40) Salmeron, M.; Schlögl, R. Ambient Pressure Photoelectron Spectroscopy: A New Tool for Surface Science and Nanotechnology. *Surf. Sci. Rep.* **2008**, *63*, 169−199.
(41) Tissot, H.; Olivieri, G.; Gallet, J.-J.; Bournel, F.; Silly, M. G.; Sirotti, F.; Rochet, F. Cation Depth-Distribution at Alkali Halide Aqueous Solution Surfaces. *J. Phys. Chem. C* **2015**, *119*, 9253−9259.
(42) Tissot, H.; Gallet, J.-J.; Bournel, F.; Olivieri, G.; Silly, M. G.; Sirotti, F.; Boucly, A.; Rochet, F. The Electronic Structure of Saturated NaCl and NaI Solutions in Contact with a Gold Substrate. *Top. Catal.* **2016**, *59*, 605−620.
(43) Tissot, H.; Coustel, R.; Rochet, F.; Boucly, A.; Carteret, C.; André, E.; Bournel, F.; Gallet, J.-J. Deciphering Radiolytic Oxidation in Halide Aqueous Solutions: A Pathway Toward Improved Synchrotron NAP-XPS Analysis. *J. Phys. Chem. C* **2023**, *127*, 15825−15838.
(44) Boucly, A.; Rochet, F.; Arnoux, Q.; Gallet, J.-J.; Bournel, F.; Tissot, H.; Marry, V.; Dubois, E.; Michot, L. J. Soft X-Ray Heterogeneous Radiolysis of Pyridine in the Presence of Hydrated

Strontium-Hydroxyhectorite and Its Monitoring by Near-Ambient Pressure Photoelectron Spectroscopy. *Sci. Rep.* **2018**, *8*, No. 6164.
(45) Coustel, R.; Boucly, A.; André, E.; Di Bitetto, A.; Bournel, F.; Gallet, J.-J.; Rochet, F.; Carteret, C. NAP-XPS Probes the Electronic Structure of the Mg-Al-Cl Layered Double Hydroxide upon Controlled Hydration. *J. Phys. Chem. C* **2021**, *125*, 4144−4153.
(46) Michot, L. J.; Villiéras, F.; François, M.; Yvon, J.; Le Dred, R.; Cases, J. M. The Structural Microscopic Hydrophilicity of Talc. *Langmuir* **1994**, *10*, 3765−3773.
(47) Rotenberg, B.; Patel, A. J.; Chandler, D. Molecular Explanation for Why Talc Surfaces Can Be Both Hydrophilic and Hydrophobic. *J. Am. Chem. Soc.* **2011**, *133*, 20521−20527.
(48) Dazas, B.; Lanson, B.; Breu, J.; Robert, J.-L.; Pelletier, M.; Ferrage, E. Smectite Fluorination and Its Impact on Interlayer Water Content and Structure: A Way to Fine Tune the Hydrophilicity of Clay Surfaces? *Microporous Mesoporous Mater.* **2013**, *181*, 233−247.
(49) Egelhoff, W. F. Core-Level Binding-Energy Shifts at Surfaces and in Solids. *Surf. Sci. Rep.* **1987**, *6*, 253−415.
(50) XPS Database. https://xpsdatabase.com/., Accessed 17 July, 2026.
(51) Komarala, E. P.; Komarala, P.; Doshi, S.; Mohammed, A.; Bahadur, D. Efficient Antibacterial Activity via Protein Degradation of a 3D Layered Double Hydroxide-Reduced Graphene Oxide Nanohybrid. *RSC Adv.* **2016**, *6*, 40389−40398.
(52) Barr, T. L.; Seal, S. Nature of the Use of Adventitious Carbon as a Binding Energy Standard. *J. Vac. Sci. Technol. A* **1995**, *13*, 1239−1246.
(53) Citrin, P. H.; Wertheim, G. K.; Baer, Y. Many-Electron Effects in Core-Level X-Ray and Electron Spectroscopies from Na, Mg, and Al. *Phys. Rev. Lett.* **1975**, *35*, 885−888.
(54) Guérin, L.; Bernhard, T.; Michot, L. J.; Ferrage, E.; Claret, F.; Marry, V. Influence of Force Field on Clay-Water Contact Angle Determination Using Molecular Dynamics. *Clays Clay Miner.* **2025**, *73*, No. e23, DOI: 10.1017/cmn.2025.8.
(55) Plimpton, S. Fast Parallel Algorithms for Short-Range Molecular Dynamics. *J. Comput. Phys.* **1995**, *117*, 1−19.
(56) Cygan, R. T.; Liang, J.-J.; Kalinichev, A. G. Molecular Models of Hydroxide, Oxyhydroxide, and Clay Phases and the Development of a General Force Field. *J. Phys. Chem. B* **2004**, *108*, 1255−1266.
(57) Berendsen, H. J. C.; Grigera, J. R.; Straatsma, T. P. The Missing Term in Effective Pair Potentials. *J. Phys. Chem. A* **1987**, *91*, 6269−6271.
(58) Fleck, M.; Wieder, M.; Boresch, S. Dummy Atoms in Alchemical Free Energy Calculations. *J. Chem. Theory Comput.* **2021**, *17*, 4403−4419.
(59) Tissot, H. Beyond the Gap of Pressure: XPS Studies of Interfaces at Near Ambient Pressures; Ph.D. thesis, Université Pierre et Marie Curie2014.
(60) Boucly, A.; Rochet, F.; Tissot, H.; Arnoux, Q.; Gallet, J.-J.; Bournel, F.; Carniato, S.; Dubois, E.; Michot, L. J.; Marry, V. Electronic Structure Sensitivity to Hydration in Smectite Clays Unveiled by Near Ambient Pressure X-Ray Photoelectron Spectroscopy. *J. Phys. Chem. C* **2024**, *128*, 17112−17123.
(61) Le Crom, S.; Tournassat, C.; Robinet, J.-C.; Marry, V. Influence of Water Saturation Level on Electrical Double Layer Properties in a Clay Mineral Mesopore: A Molecular Dynamics Study. *J. Phys. Chem. C* **2022**, *126*, 647−654.
(62) Le Crom, S.; Tournassat, C.; Robinet, J.-C.; Marry, V. Influence of Polarizability on the Prediction of the Electrical Double Layer Structure in a Clay Mesopore: A Molecular Dynamics Study. *J. Phys. Chem. C* **2020**, *124*, 6221−6232.
(63) Vantelon, D.; Belkhou, R.; Bihannic, I.; Michot, L. J.; Montargès-Pelletier, E.; Robert, J.-L. An XPEEM Study of Structural Cation Distribution in Swelling Clays. I. Synthetic Trioctahedral Smectites. *Phys. Chem. Miner.* **2009**, *36*, 593−602.
(64) Fang, Y.; Zhao, C.-B.; Gong, Z.-M.; Wang, S.-P.; Ye, X.-Q.; Pan, Q.-F.; Li, G.; Cui, Y.; Yao, Y.-X.; Luo, W.-H. In Situ NAP-XPS Study of CO_2 and H_2O Adsorption on Cerium Oxide Thin Films. *Chem. Phys. Lett.* **2022**, *794*, No. 139496.
(65) Byrne, C.; Zahra, K. M.; Dhaliwal, S.; Grinter, D. C.; Roy, K.; Garzon, W. Q.; Held, G.; Thornton, G.; Walton, A. S. A Combined Laboratory and Synchrotron In Situ Photoemission Study of the Rutile TiO_2(110)/Water Interface. *J. Phys. D: Appl. Phys.* **2021**, *54*, No. 194001.
(66) Vujin, J.; Huang, W.-X.; Ciganovic, J.; Ptasinska, S.; Panajotovic, R. Direct Probing of Water Adsorption on Liquid-Phase Exfoliated WS_2 Films Formed by the Langmuir-Schaefer Technique. *Langmuir* **2023**, *39*, 8055−8064.
(67) Smith, D. E.; Dang, L. X. Computer Simulations of NaCl Association in Polarizable Water. *J. Chem. Phys.* **1994**, *100*, 3757−3766.
(68) Dang, L. X. Mechanism and Thermodynamics of Ion Selectivity in Aqueous Solutions of 18-Crown-6 Ether: A Molecular Dynamics Study. *J. Am. Chem. Soc.* **1995**, *117*, 6954−6960.
(69) Malikova, N.; Cadène, A.; Dubois, E.; Marry, V.; Durand-Vidal, S.; Turq, P.; Breu, J.; Longeville, S.; Zanotti, J.-M. Water Diffusion in a Synthetic Hectorite Clay Studied by Quasi-Elastic Neutron Scattering. *J. Phys. Chem. C* **2007**, *111*, 17603−17611.
(70) Dazas, B.; Jiménez-Ruiz, M.; Grégoire, B.; Hubert, F.; Lanson, B.; Tertre, E.; Michot, L. J.; Ferrage, E. Molecular Hydrophobicity Signature in Charged Bidimensional Clay Materials. *J. Phys. Chem. A* **2024**, *128*, 10358−10371.
(71) Bérend, I.; Cases, J.-M.; François, M.; Uriot, J.-P.; Michot, L. J.; Masion, A.; Thomas, F. Mechanism of Adsorption and Desorption of Water Vapor by Homoionic Montmorillonites: 2. The Li^+, Na^+, K^+, Rb^+ and Cs^+ Exchanged Forms. *Clays Clay Miner.* **1995**, *43*, 324−336.
(72) Chatterjee, A.; Ebina, T.; Onodera, Y.; Mizukami, F. Effect of Exchangeable Cation on the Swelling Property of 2:1 Dioctahedral Smectite: A Periodic First Principle Study. *J. Chem. Phys.* **2004**, *120*, 3414−3424.
(73) Rinnert, E. Etats d'hydratation d'argiles suivis par analyses vibrationnelles de l'eau et des hydroxyles dans le proche infrarouge: Application aux systèmes saponite et bentonite; Ph.D. thesis, Université de Lorraine2004.
(74) Raman, A. S.; Selloni, A. Insights into the Structure and Dynamics of K^+ Ions at the Muscovite-Water Interface from Machine Learning Potential Simulations. *J. Chem. Phys.* **2024**, *160*, No. 244708.
(75) Tesson, S.; Salanne, M.; Rotenberg, B.; Tazi, S.; Marry, V. Classical Polarizable Force Field for Clays: Pyrophyllite and Talc. *J. Phys. Chem. C* **2016**, *120*, 3749−3758.
(76) Tesson, S.; Louisfrema, W.; Salanne, M.; Boutin, A.; Rotenberg, B.; Marry, V. Classical Polarizable Force Field to Study Dry Charged Clays and Zeolites. *J. Phys. Chem. C* **2017**, *121*, 9833−9846.
(77) Narayanan Nair, A. K.; Cui, R.; Sun, S. Overview of the Adsorption and Transport Properties of Water, Ions, Carbon Dioxide, and Methane in Swelling Clays. *ACS Earth Space Chem.* **2021**, *5*, 2599−2611.
(78) Zhang, C.; Wang, J.; Chen, R. Water Adsorption Isotherms on Soil External Particle Surface by Molecular Simulation. *Comput. Geotech.* **2021**, *139*, No. 104432.
(79) Tesson, S.; Louisfrema, W.; Salanne, M.; Boutin, A.; Ferrage, E.; Rotenberg, B.; Marry, V. Classical Polarizable Force Field to Study Hydrated Charged Clays and Zeolites. *J. Phys. Chem. C* **2018**, *122*, 24690−24704.